Remotely sensed and field surveyed early-warning signals of desertification in the Ebro basin, Spain

by

J.H. den Daas

First Supervisor: dr. D.J. Karssenberg

Second Supervisor: dr. Y. Pueyo Estaún

Second Reviewer: prof. dr. S.M. de Jong

Final version

January 2018

Department of Physical Geography, Utrecht University

Abstract

The Ebro Basin near Zaragoza, Spain is the northern most semi-arid region in Europe with shrubland vegetation, a large water deficit and high grazing pressure in the last century. Early warning signals of desertification in the form of spatial and temporal variation in vegetation cover derived using remote sensing and field measurements were studied. They may provide enough time to act before a critical shift to a barren state induced by overgrazing in semi-arid zones takes place. Vegetation cover derived using a spectral mixture analysis from 18 Landsat images (1984-2008) was used to calculate spatial variation using the coefficient of variation (C_v) with a 5x5 moving window. Temporal variation was calculated using a moving window of 5 images. Vegetation cover showed a significant moderate correlation with spatial variation (-0.49) and temporal variation (-0.35). 80% of the study area showed this negative relationship. Differences in the mean of the environmental factors slope, aspect and vegetation cover show differences between these areas and itself could influence the relationship between early warning signal and vegetation cover. Early warning signals were also measured in the field using the line intercept method in 24 500m transects. Spatial variation again showed a moderate correlation (-0.46) with vegetation cover. Remotely sensed spatial variation correlated with spatial variation measured in the field (0.47). This shows that the early warning signals spatial and temporal variation can possibly contribute to remotely mapping of desertification.

Acknowledgements

I want to thank Derek for his guidance and insights during the process of writing this thesis. Yolanda and her colleagues at IPE-CSIC in Zaragoza helped me immensely in getting acquainted with the area and their research using field transects and made me feel welcome. Steven thank you for taking the time out of your busy schedule to review this thesis.

Contents

1. Introduction

The importance of drylands to the food security of large parts of the global population was demonstrated by droughts in the last few decades. Millions of people were and are still affected by desertification (Dregne et al., 1991). The Sahel droughts and famines in the 1970s are a good example. Desertification can be caused by an increase in grazing pressure. Small changes in the load of grazing can cause a total shift to a barren state once a critical threshold is passed (Scheffer et al., 2001). There was a call for improved prediction of these shifts after the Sahel droughts (Westing, 1994). Early warning signals derived from statistical properties of vegetation cover might provide ample time to prevent a critical shift induced by overgrazing in semi-arid zones (Karssenberg and Bierkens, 2012).

The theory of critical shifts and early warning signals in ecosystems can contribute to remotely mapping of desertification (Scheffer et al., 2001, 2009, 2012). Thus far, the existence of early warning signals of critical shifts in ecosystems has mainly been proven in model studies (Kéfi et al., 2007; Guttal and Jayaprakash, 2008; Dakos et al., 2009; Karssenberg and Bierkens, 2012). Occurrence in the field should be determined but early warning signals have not been effectively measured in the field. There have been some studies using field experiments or observations but their main focus was on vegetation patterns (Rietkerk et al., 2004; Kéfi et al., 2007, 2014). Most remote mapping of desertification is done observing change in biomass using rain use efficiency (RUE) or similar indicators instead of early warning signals (Munyati and Makgale, 2009; Paudel and Andersen, 2010; Vicente-Serrano et al., 2012; Fensholt et al., 2013). Karssenberg and Bierkens (2012) concluded that the use of spatial and temporal variance were better early warning signals than mean biomass. There is a lack of empirical data of spatial early warning signals and temporal indicators (Kéfi et al., 2014). Early warning signals for desertification can be measured using remote sensing and field measurements. This study will aim to determine if early warning signals occur in the field using both remote sensing and field measurements and answer the following questions;

- Can early warning signals contribute to remotely mapping of desertification?
    - Can remotely sensed spatial and temporal variation of vegetation cover be used as early warning signals of desertification?
    - Are remotely sensed early warning signals of desertification dependent on environmental factors?
    - Can early warning signals of desertification be measured in the field?
    - How are remotely sensed early warning signals related to early warning signals measured in the field?

The study area lies in the Ebro Basin near Zaragoza, Spain which is the northern most semi-arid region in Europe with a large water deficit and high grazing pressure in the last century. It shows a trend of decreasing vegetation cover under water stress conditions even during a period of decreasing grazing pressure in the last decade (Vicente-Serrano et al., 2012). This makes it suitable for studying early warning signals of critical shifts in desertification. The theory behind desertification, critical shifts and early warning signals are covered in the following introductory chapters as well as an outline of the study area. The methodology and results were split up in chapters for remotely sensed and field measured early warning signals.

2. Background

2.1. Desertification

Thirty percent of the world's land surface suffers from desertification (Dregne et al., 1991). Desertification is defined as 'land degradation in arid, semi-arid and dry sub-humid areas resulting from various factors, including climatic variations and human activities' (UNCED, 1992). Significant desertification can be prevented in two thirds of the regions at risk if the maximum global warming level is limited to 1.5 °C (Park et al., 2018). These areas have between 0–300 mm precipitation per year and are characterised by drought, low and variable rainfall and high temperature and evaporation (FAO, 1987). The interest in desertification was sparked by the droughts in the African Sahel in the 1970s, for the first time satellite photos could show the human impact on the land (Nicholson et al., 1998). Ecological frailty is one of the causes of desertification, which is related to limited water resources, the variability of rainfall, thin plant cover and poor soils (Kassas, 1995). However, desertification in arid and semi-arid zones can primarily be contributed to the over utilization of resources and insufficient land management (Li et al., 2000). The driving forces behind this are increased population and the transition from sustenance farming to farming for export (Kassas, 1995). These changes bring about growing livestock numbers, overcultivation, intensive irrigation and deforestation (Nicholson et al., 1998). Livestock grazing is more intensive close to watering points and therefore these areas will be more degraded, a piosphere, which decreases with distance (Jafari et al., 2008). Animals grazing near watering points also makes the land more impacted by wind and water erosion (Nicholson et al., 1998). In Europe desertification processes affect the Mediterranean and the Central and Eastern European countries (Montanarella and Tóth, 2008).

2.2. Critical Shifts and Early Warning Signals

Critical shifts are large sudden changes in the structure and functioning of a system (Biggs et al., 2009). Desertification as the complete loss of vegetation is such a transition (Scheffer et al., 2009). The behavior of such a change in an ecosystem is explained by Scheffer et al. (2001). External conditions on a system such as the climate, grazing and harvest often change gradually with time. A system can change sudden from one stable situation to another when a critical boundary in external conditions has been surpassed. To restore the previous conditions, the system needs to recover past the external conditions of the critical shift (Scheffer et al., 2009). This means more effort is needed in reversing the critical shift than is needed to prevent it, in this study from a barren state back to a vegetative state.

Thus, detecting beforehand if a system is approaching a critical shift is useful, because it allows acting to prevent the actual shift to unfold. Scheffer et al. (2009) described the concept of critical slowing down as a possible early warning signal. A system close to a critical shift is more susceptible to forcing and small fluctuations can lead to a large change in state. This means that fluctuations are larger near the tipping point. In arid ecosystems this might be exhibited by the patchiness of the vegetation (figure 2.2.1) (Rietkerk et al., 2004). Different patterns such as gaps, labyrinths stripes and spots are self-organized by the system. Dakos et al. (2009) suggest that an increase in spatial correlation is a leading indicator for an impending critical shift. Kéfi et al. (2007) modelled the relation between the spatial organization of the

vegetation and the amount of external stress. The patch size distribution of the vegetation follows a power law, which is deviated from close to the critical shift. Therefore, this might be an early warning signal for desertification. Karssenberg and Bierkens (2012) found that the use of spatial and temporal variance in biomass collected from modelled samples as early warning signals reduces the uncertainty of the forecasted timing of the critical shift. However, a dense sampling network is needed to make the early warning signal useful. Dakos et al. (2009) had better results when using spatial correlation as early warning signals compared to temporal indicators. Tirabassi et al. (2014) assessed the quality of different early warning indicators and found that distribution based indicators have a high value. The coefficient of variation C_v has been successfully used as early warning signal of critical shifts in population studies (Balbontín et al., 2003; Drake and Griffen, 2010; Carpenter et al., 2011). C_v as measure of spatial variation is expected to increase when nearing a critical shift. There was some success using spatial variation in the form of the moving standard deviation index (MSDI) (using a 3x3 moving window on the third Landsat band) to remotely asses land degradation (Tanser and Palmer, 1999; Guo et al., 2004; Jafari et al., 2008; Xu et al., 2009). Karssenberg et al. (2017) suggest that direct evidence of transitions between states in semi-arid ecosystems can be provided using remote sensing data.

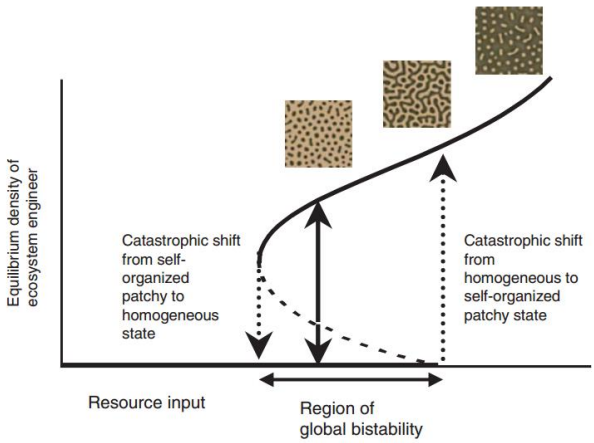

Figure 2.2.1. Sequence of self-organizing vegetation patches towards a critical shift. Resource input can also be grazing pressure. Taken from Rietkerk et al., 2004.

2.3. Study area

The study area is part of the Ebro basin located in the Aragón region in Spain (figure 2.3.1.). It is the northernmost semi-arid region in Europe as well as one the most arid regions of the Iberian Peninsula (Vicente-Serrano et al., 2012). The area experiences droughts that have increased in frequency in the last century (Vicente-Serrano and Cuadrat-Prats, 2006) Most of the south facing slopes below 1600 m were cultivated until 1970 (López-Moreno et al., 2011). By 1970 most were abandoned due to poor productivity and policy from the European Community (Vicente-Serrano et al., 2012). While the farming induced land degradation, land abandonment in these areas caused regrowth of shrubs and in some places induced afforestation (Vicente-Serrano et al., 2004). The dominant land uses are steppes and dry farming areas with herbaceous cultivations (Vicente-Serrano et al., 2006) (figure 2.2.1). Low vegetation cover is caused by the low water availability, poor soils and droughts (Vicente-Serrano et al., 2004). The water deficit is mainly caused by a high potential evapotranspiration and the soils are low in nutrients and organic matter due to the lithology (Vicente-Serrano et al., 2012). The lithology mostly consists of gypsum and carbonate deposits (Soriano et al., 1994). The average annual precipitation is about 320 mm with most rainfall in spring and autumn (Agencia Estatal de Meteorología, 2016). In the summer the average temperature during the day surpasses 30 °C and during winters reaches 10 °C on average.

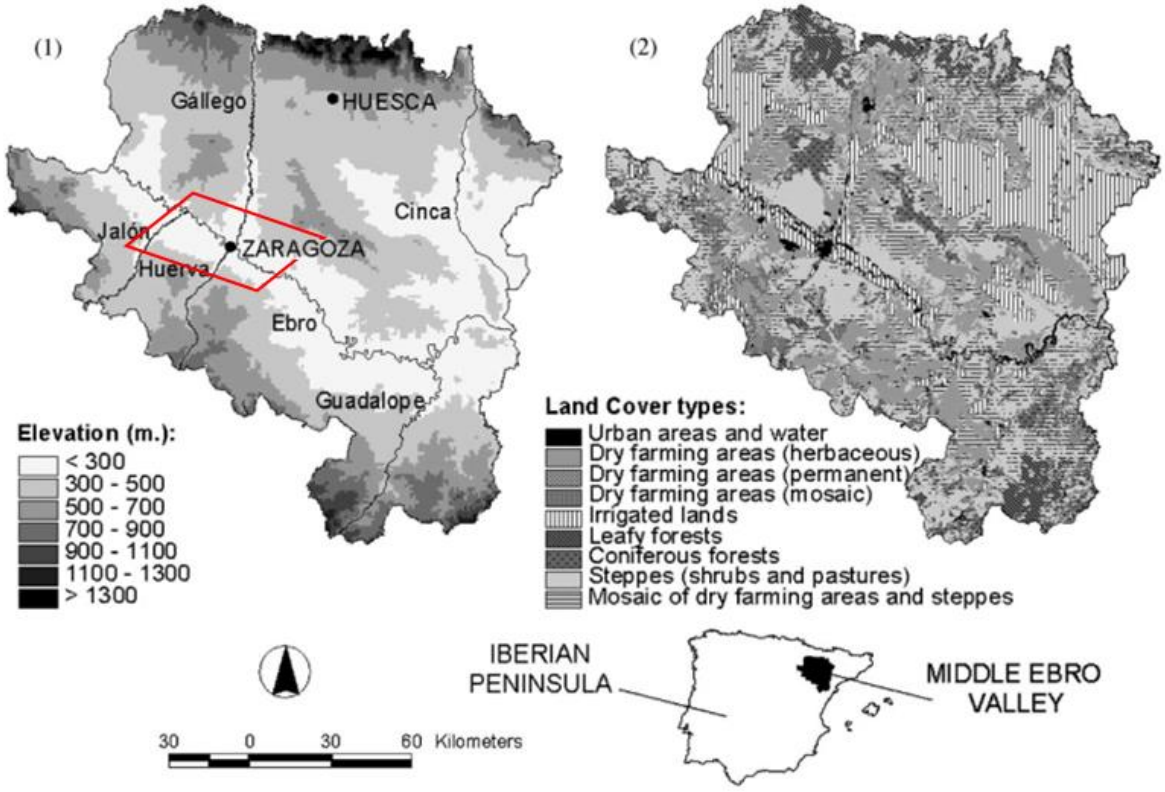

Figure 2.3.1 Elevation (1) and land cover map (2) of the study area (in red) within Ebro basin, Spain. Taken from Vicente-Serrano et al., 2006.

3. Methods

To determine if early warning signals of desertification can contribute to remotely mapping of land degradation remote sensing data from a dryland area in Europe, the Ebro basin, was used. Early warning signals were calculated using both temporal and spatial variation and then correlated to vegetation cover (figure 3.1.). Vegetation cover was used as a proxy for desertification because it is a good indicator and easier to assess using satellite images than other indicators of desertification such as erosion. (Nicholson et al., 1998; Symeonakis and Drake, 2004). To determine the influence of environmental factors on the early warning signals trends over time of variation and cover were combined and classified. Spatial variation was also calculated for the field transects to determine if early warning signals can also be measured in the field.

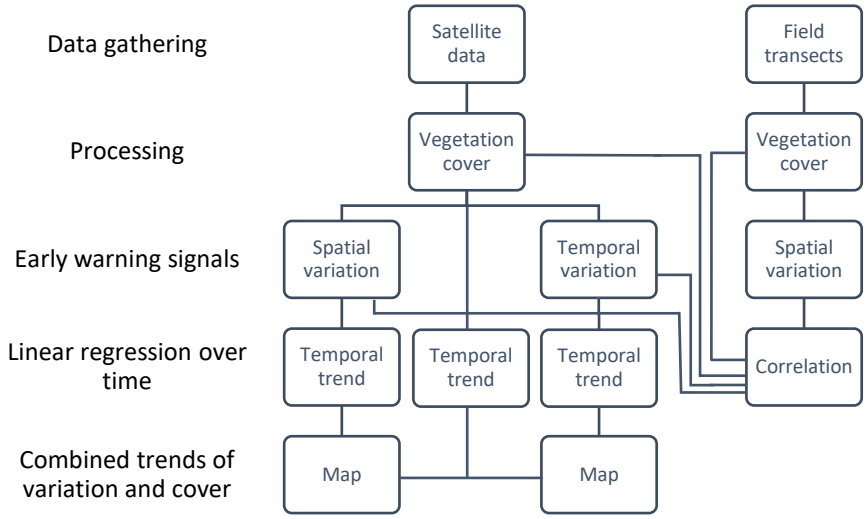

Figure 3.1. Scheme of methodology

3.1. Remote Sensing

3.1.1 Satellite data

The satellite data was obtained from the Landsat program which collects data in up to seven spectral bands between the visible light and thermal infrared. The program provides data from 1975 to the present and is therefore suitable to assess slow processes as desertification. The spatial resolution of Landsat data is 30 meters, which is suitable for an assessment on a medium to small scale. The data set used by Vicente-Serrano et al. (2012) comprising 18 processed cross-calibrated images of Landsat 5-TM and Landsat 7-ETM+ between 1984 and 2009 was used (Table 3.1.1.). The processing and calculations on these images were done using the Google Earth Engine which provides the tools and public data needed to perform analysis and computations of satellite data (Gorelick et al., 2017).

Table 3.1.1. Satellite images used to study desertification

Date of acquisition	Satellite	Sensor
1984-08-20	Landsat 5	TM
1985-08-07	Landsat 5	TM
1987-08-13	Landsat 5	TM
1989-08-02	Landsat 5	TM
1991-08-24	Landsat 5	TM
1992-08-10	Landsat 5	TM
1993-08-29	Landsat 5	TM
1995-08-03	Landsat 5	TM
1997-08-24	Landsat 5	TM
1999-08-14	Landsat 5	TM
2000-08-08	Landsat 7	ETM
2001-07-26	Landsat 7	ETM
2002-08-30	Landsat 7	ETM
2004-08-27	Landsat 5	TM
2005-08-14	Landsat 5	TM
2006-08-01	Landsat 5	TM
2007-08-04	Landsat 5	TM
2008-08-06	Landsat 5	TM

3.1.2 Relation between remotely sensed early warning signals and vegetation

Two indicators for vegetation were used, the Normalized Difference Vegetation Index (NDVI and vegetation cover from a Spectral Mixture Analysis (SMA) performed by Vicente-Serrano et al. (2012). Both can be derived from remotely sensed data. The NDVI was calculated using:

$$NDVI = \frac{NIR - RED}{NIR + RED} \qquad [1]$$

Where RED is the Red band and NIR is the Near infrared band of the satellite images.

Vegetation cover obtained with the SMA instead of the NDVI may provide better result in drylands with patchy shrub vegetation (Elmore et al., 2000). The endmembers of the shrubs and the bare soil were used to calculate the vegetation cover using least squares (equation 2.1 and 2.2). The sum of the fractions for vegetation cover and bare soil were assumed to be one for each pixel (Vicente-Serrano et al., 2012). To ensure that the analysis is applied only on shrublands and bare soil, a mask made by Vicente-Serrano et al. (2012) was applied on the collection of images. This mask was based on a land cover map, the Spanish National Forestry Map, and the geological map of Aragón (MAPA, 1978; MMA, 2006; SITAR, 2007)

$$P\lambda = \sum_{j=1}^{n} F_j \times P_{\lambda,j} + E_\lambda \quad [2.1]$$

$$\sum_{j=1}^{n} F_j = 0 \qquad [2.2]$$

Where P_λ is the reflectance of band λ, F_j is the percentage of the endmember *j*, $P_{\lambda,j}$ is the reflectance of the endmember *j* in band 1, *n* is the number of endmembers, and E_λ is the residual error in band λ (Vicente-Serrano et al., 2012).

The coefficient of variation C_v was used as early warning signal. It was applied to both the NDVI and vegetation cover calculated using SMA.

$$C_v = \frac{\sigma}{\mu} \qquad [3]$$

Where μ is the mean and σ the standard deviation of the set of values used to calculate the coefficient of variation C_v.

The coefficient of variation was calculated both spatially and temporally. The spatial variation was calculated for each pixel and each image using a moving 5x5 square window with a stride of one (figure 3.1.1.). Smaller windows could amplify the differences within the moving window and increase noise (Lu and Batistella, 2005). The MSDI is calculated using the standard deviation of a 3x3 window on the third band to compare against C_v as early warning signal.

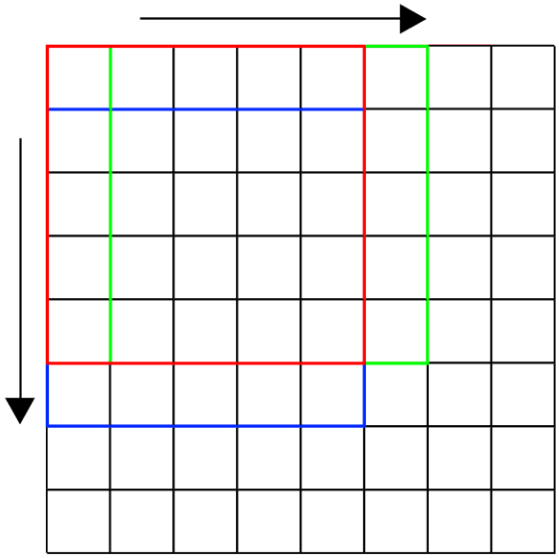

Figure 3.1.1. Square 5x5 moving window. Arrows indicate direction of movement.

Temporal variation was calculated for each pixel using a moving window of 5 years. This includes the 4 previous and current year the variation is calculated for (figure 3.1.2.). This is done to be able to calculate an early warning signal for the current year. This produces 18 maps of spatial variation one for each year. Fourteen maps of temporal variation were created for the years 1991-2008 as 1991 is the first year with 4 preceding images to use in the moving window.

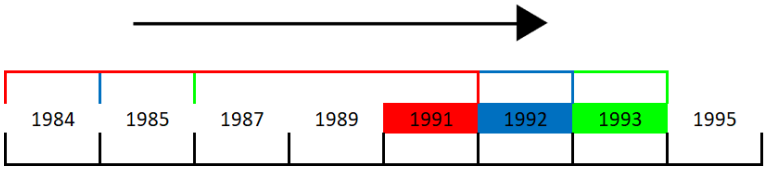

Figure 3.1.2. 5 year moving window. Arrow indicates direction of movement.

Both spatial and temporal C_v were correlated with vegetation cover and NDVI on a per pixel (location) basis based on the timeseries of the pixel (n=18). The overall correlation between these factors was also calculated using the 2008 image. Plots were made using a random sample of 79400 pixels from 2008 for the whole area.

3.1.2 Temporal trends

The temporal trend in the variables NDVI, cover, C_v (temporal), C_v(spatial) was assessed by running a linear least squares regression. For the timeseries of every pixel the slope of the fitted line was calculated. The value for a pixel is calculated using the timeseries of that pixel from the multiple images in the dataset (figure 3.1.3.).

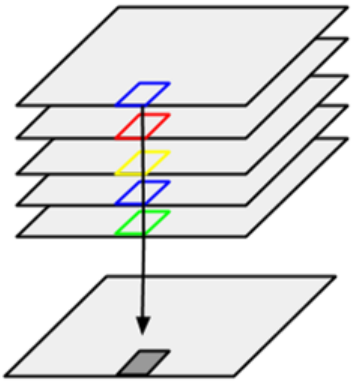

Figure 3.1.3. Google Earth Engine reducer (Google, 2010).

3.1.3 Classification of combined temporal trends of vegetation cover and variation

To test if increased spatial variation indicates a system closer to collapse, the temporal trends in vegetation cover were combined with temporal trends in spatial and temporal C_v. Four different situations are possible when comparing temporal trends in vegetation cover and C_v. Two classes would have a negative relationship and two have a positive relationship over time between vegetation and C_v (figure 3.1.4.).

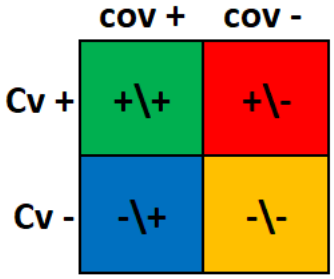

Figure 3.1.4. Four possible classes that are different regarding positive (+) and negative (-) temporal trends of vegetation cover (cov) and variation (Cv) over time.

The values of the environmental factors slope (USGS, 2006), aspect, vegetation cover and height above nearest drainage (HAND (Nobre et al., 2011)) were compared to study the differences between the classes in figure 3.1.4. Boxplots were made using the values for the environmental factors and class extracted using the random sample mentioned above.

3.2. Field data

3.2.1 Relation between early warning signals and vegetation in the field

In the field vegetation cover was assessed. Vegetation cover can be inferred from transects using the line-intercept method, where the length of patches along the transect is measured (Kéfi et al., 2007). When the transect length that is covered with vegetation is divided by the total length the vegetation cover can be obtained. To assess vegetation cover in the field 24 500m transects with an intercept distance of 20 cm from a field survey conducted by Pueyo et al. (2013) in the summer of 2010 were used. The transects were taken in 8 different locations in grazed and ungrazed conditions (figure 3.2.1). For this study field measurements were also taken and have been used to test some theories but were not suitable for this study. The vegetation cover was compounded to cells of 10m. Spatial variation of vegetation cover was calculated using the coefficient of variation using a moving window along the transects of 5 cells (50m). The correlation between spatial C_v and vegetation cover was calculated.

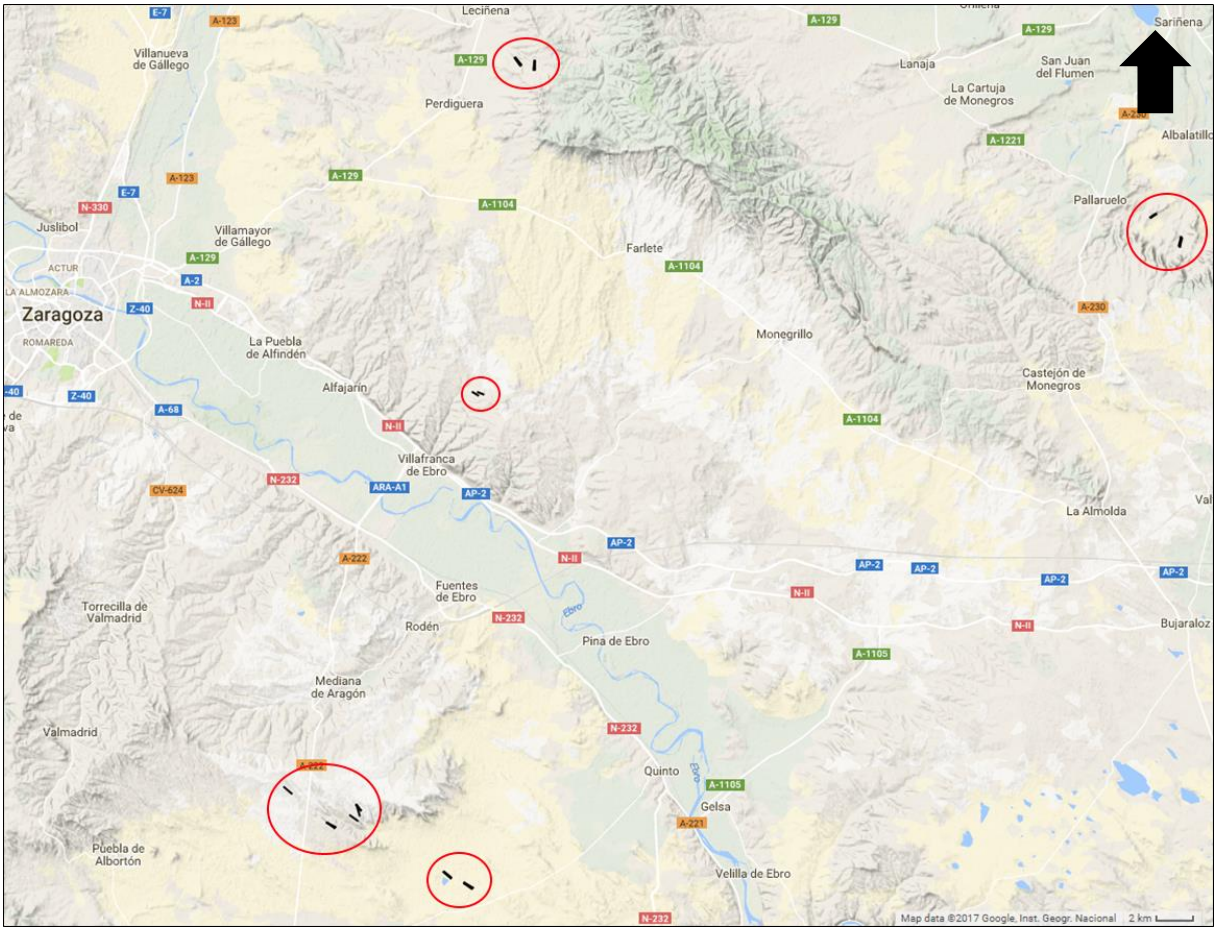

Figure 3.2.1. The 24 Transects (in the red circles) used to estimate vegetation cover.

3.2.2 Comparing field surveyed to remotely sensed early warning signals

The 24 transects were split in two creating 48 250 meter transects. Over these 250 meters the average vegetation cover and spatial variation were calculated. The location of these 48 points was used to extract the remotely sensed spatial C_v, MSDI and NDVI from a 2010 Landsat image (taken 25-04) separate from the dataset in table 3.1.1. The remotely sensed data was then compared and correlated with the field data.

4. Results

4.1. Remote sensing

4.1.1 Relations between remotely sensed early warning signals and vegetation

The early warning signals spatial and temporal C_v calculated using vegetation cover from the spectral mixture analysis were compared with the vegetation cover to asses their suitability as early warning signals of desertification. The descriptive statistics of the random sample taken from the 2008 satellite image are in Table 4.1.1.

Table 4.1.1. Descriptive statistics of vegetation cover (fraction calculated using Spectral Mixture Analysis), NDVI, spatial and temporal C_v (no units) (using cover) (n=79400).

	Cover	NDVI	Spatial C_v	Temporal C_v	MSDI
Min	0.01	-0.022	0.077	0	0.033
Mean	0.240	0.243	0.325	0.265	0.163
Max	1	0.775	1.099	1.410	0.652
Stdev	0.11	0.06	0.11	0.14	0.051

Plots were made, and the Pearson correlation was calculated (n=79400) to study this) relationship (figure 4.1.1.). Descriptive statistics are in table 4.1.1. NDVI and cover show a very linear relation and have a very high correlation coefficient (0.91). There was a strong to moderate negative correlation (-0.49) between cover and spatial C_v and a moderate negative correlation (-0.35) between temporal C_v and cover. The MSDI however shows a moderate positive correlation (0.29). All correlations were significant (p-value < 0.001). The Pearson correlation calculated on a per pixel (location) basis (n=18, i.e. 18 years) showed that spatially 82% of the locations had a negative correlation between spatial C_v and vegetation cover, while 78% of the study area had a negative correlation between temporal C_v and vegetation cover.

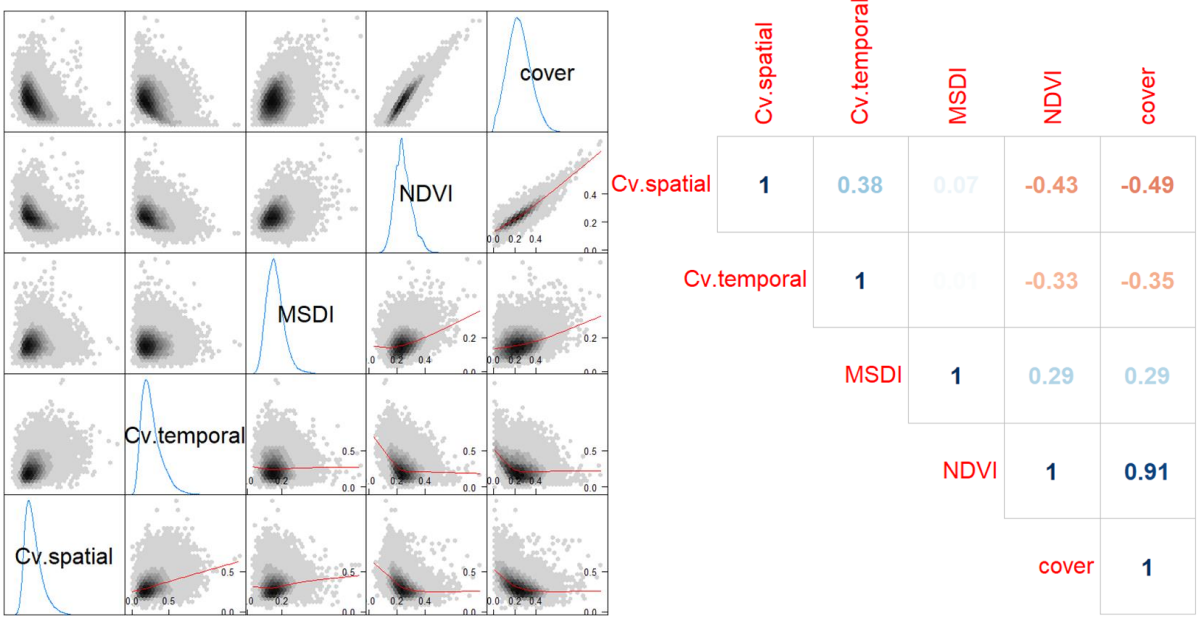

Figure 4.1.1. Hexagon scatterplot (left) and correlation matrix (right) between vegetation cover, NDVI, temporal and spatial C_v (using vegetation cover from the Spectral Mixture Analysis) (n=79400).

The Pearson correlation was also calculated for NDVI and the spatial C_v and temporal C_v calculated from NDVI. There was a weak negative correlation (-0.13) between NDVI and spatial C_v and very weak correlation with temporal C_v (0.06). However, all correlations were still significant (p-value < 0.001). The NDVI seems less suited to calculate spatial C_v and temporal C_v due to the weak correlations. This result and the high correlation between cover and NDVI was the reason the subsequent maps were created using vegetation cover only.

4.1.2 Temporal trends

To study the spatial distribution of trends over time of cover, spatial C_v and temporal C_v a linear regression was run. The linear regression resulted in three maps showing the slope (negative or positive) of the fitted line. The map created of the vegetation cover over time shows that major part of the area had a decrease in vegetation cover. However, there are larger areas to the south of Zaragoza that showed a positive trend in vegetation cover.

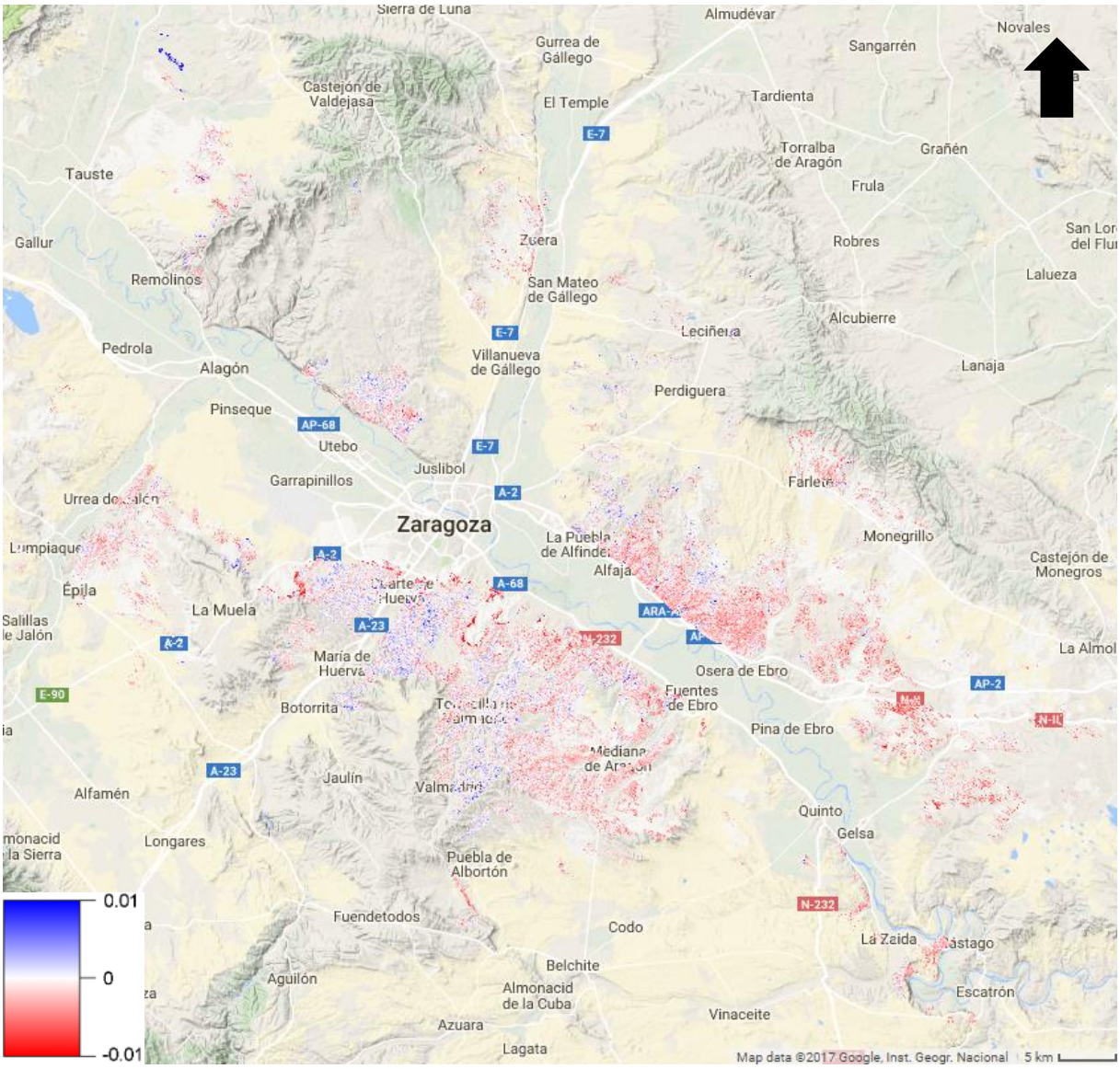

Figure 4.1.2. Slope of the line fitted to vegetation cover over time (1984-2008).

The map created of the spatial C_v shows a very uniform trend, most of the area had a slight increase of spatial C_v (Figure 4.1.3). There are some areas that had a small decrease. The map created of the temporal C_v shows a more heterogenous image. Most of the pixels had an increase of temporal C_v, but there are a lot of pixels with an increase in temporal C_v scattered through the area as well as pixels that did not increase or decrease.

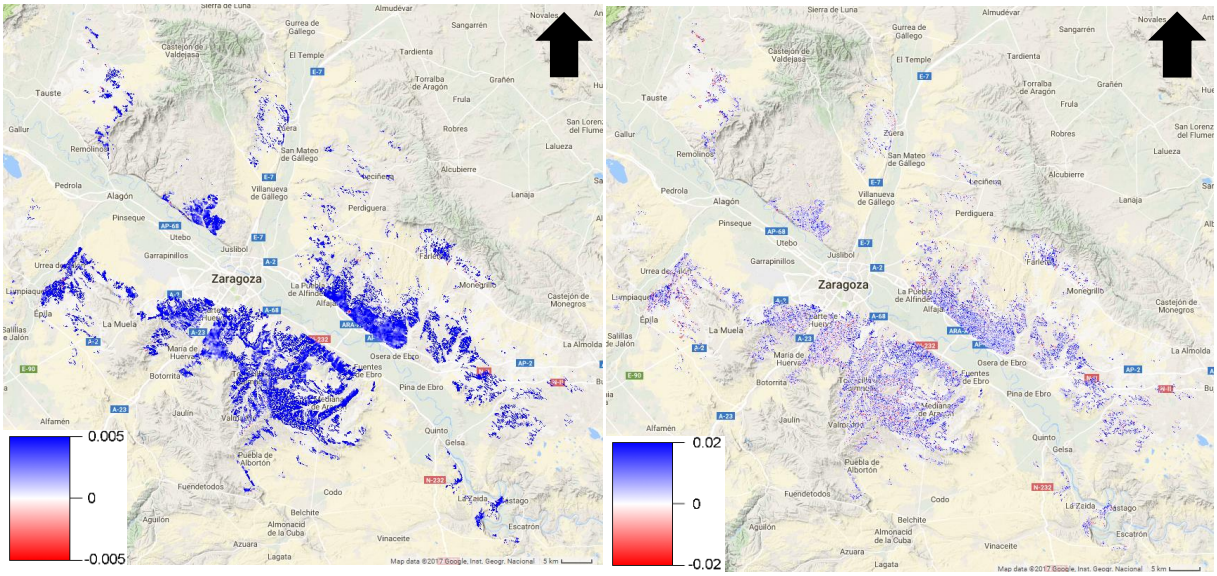

Figure 4.1.3. Slope of the line fitted to spatial C_v (left) and temporal C_v(right) over time (1984-2008).

4.1.3 Classification of combined temporal trends of vegetation cover and variation

To study the spatial relationship between the early warning signal spatial C_v and vegetation cover their trends were combined to create four classes (figure 4.1.3.). Areas are spatially congregated. The first class has the largest area, shows a decrease in cover, increase of spatial C_v and is located mainly east and southeast of Zaragoza. The fourth, the second largest, has an increase in both vegetation cover and spatial C_v and is mainly located south of Zaragoza. East of Zaragoza river small areas of green seem to follow the channels. South of Zaragoza the green areas seem to inhabit only one part of the slopes. The other two classes with a decrease in spatial C_v seem to be due to human influences of new buildings and cleared areas when visually inspecting these areas on recent high-resolution satellite images in Google Earth.

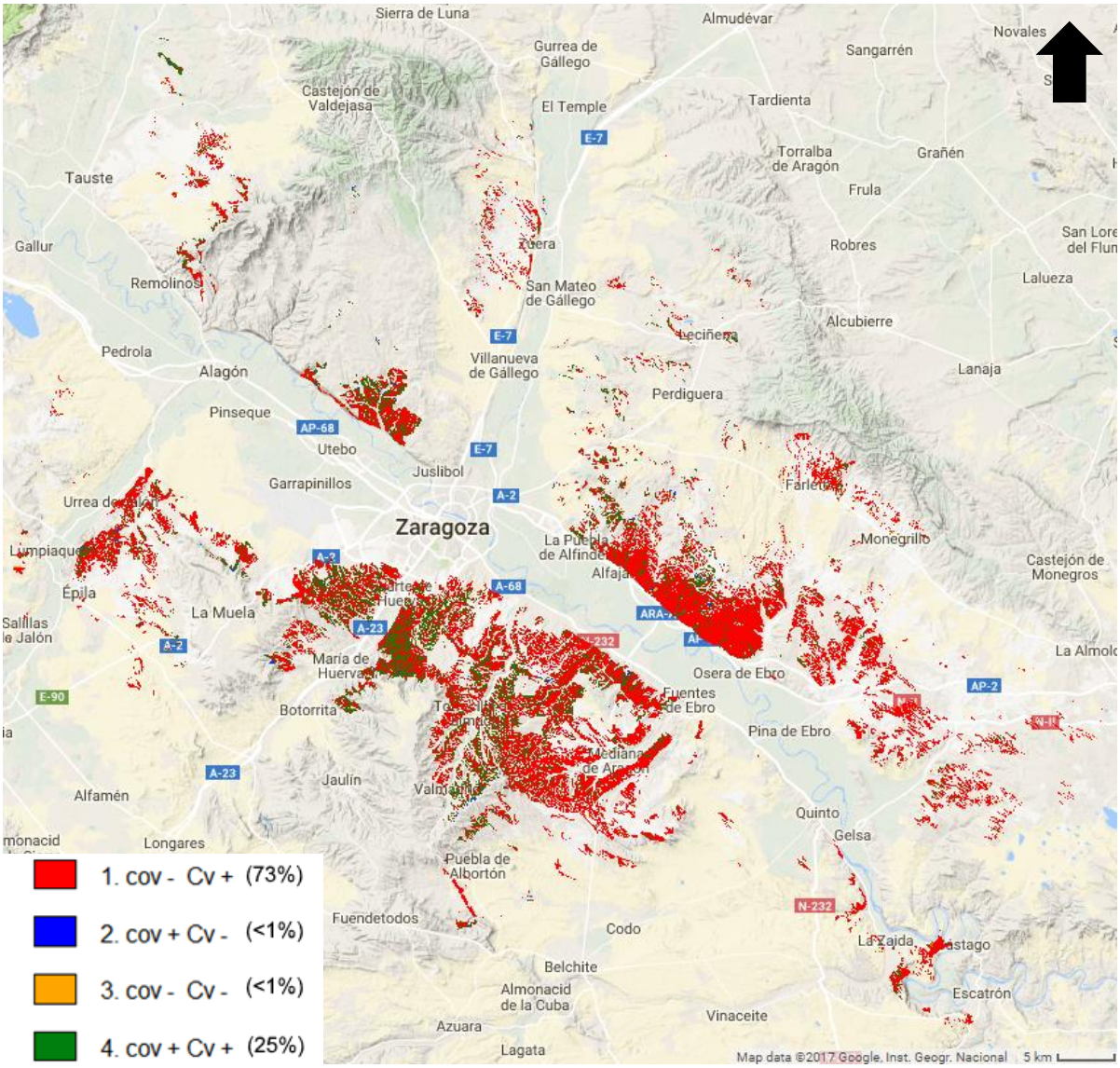

Figure 4.1.4. Four classes of combined increasing (+) or decreasing (-) temporal trends of vegetation cover (cov) and spatial C_v. Percentages of the total area are indicated between brackets for each class.

The trends in vegetation cover and temporal C_v over time were also combined to create four classes (figure 4.1.5.) In the spatial distribution of trends in vegetation cover and temporal C_v there is somewhat more variation (figure 4.1.4.). The first class with the largest area and a decline in vegetation cover and an increase in temporal C_v dominates the area east of Zaragoza. Large parts south of Zaragoza had a decrease in vegetation cover with either an increase or decrease of temporal C_v. The third class with both a decrease in temporal C_v and vegetation cover is scattered throughout the area but seems to be congregated in the most western part of the study area and southeast of Zaragoza.

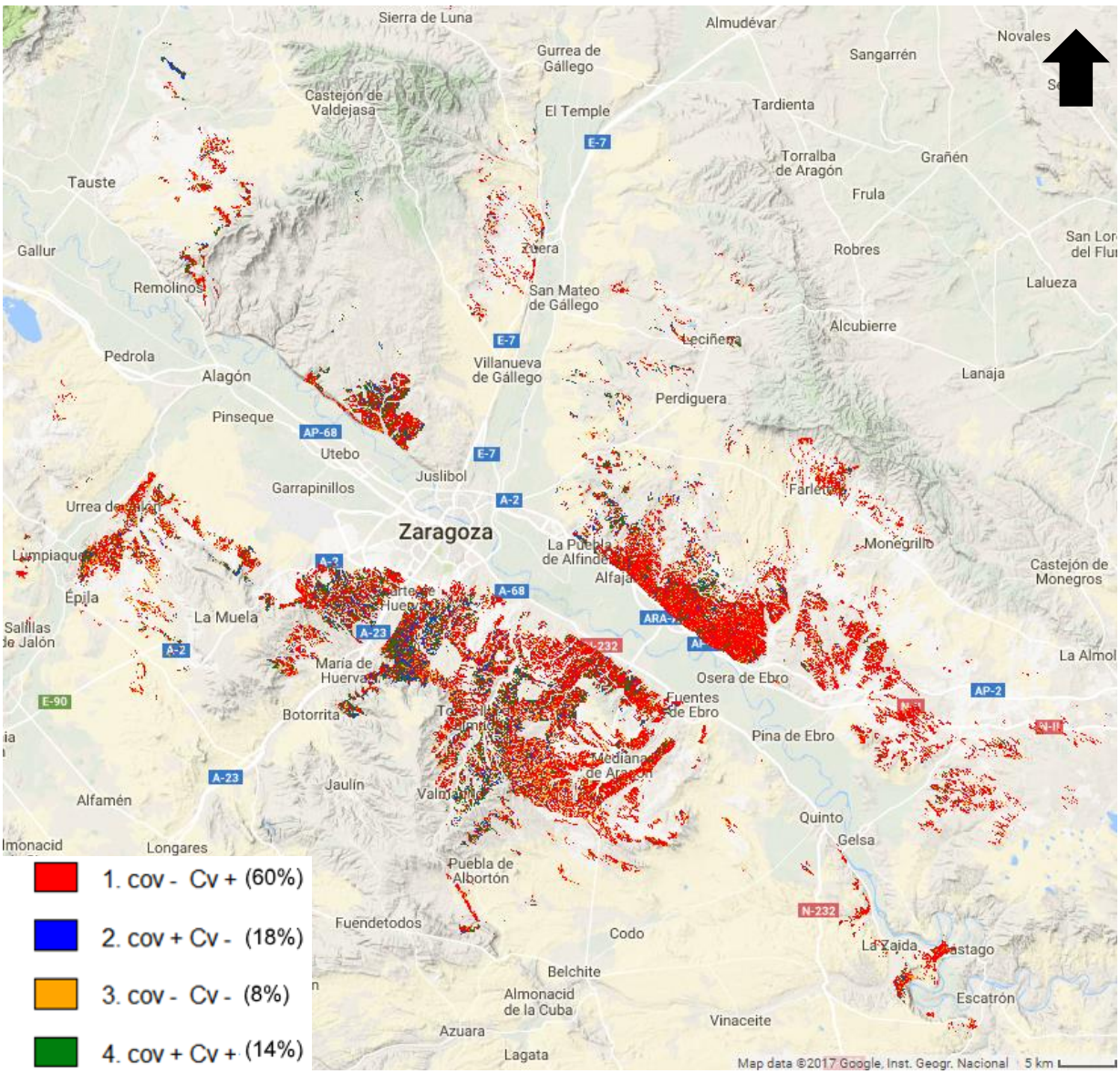

Figure 4.1.5. Four classes of combined increasing (+) or decreasing (-) temporal trends of vegetation cover (cov) and temporal C_v. Percentages of the total area are indicated between brackets for each class.

4.1.4 Environmental factors

To study the influence of environmental factors on the spatial distribution of combined temporal trends in the early warning signal spatial C_v and vegetation cover a boxplot was made for each factor and each class (figure 4.1.6.). Of all environmental factors, vegetation cover has the largest influence on the combined trends in C_v and cover. Classes with a positive relationship between cover and spatial CV (classes 3 and 4) are found in areas with relatively high cover. Differences in mean and max slope can also be seen between the classes. Especially the class with a decrease in both cover and spatial C_v (3) has a higher mean and max slope compared to the other classes. The classes with a positive relationship between cover and spatial C_v (3 and 4) show a higher mean Aspect than the other two. The HAND values are similar in mean and min/max.

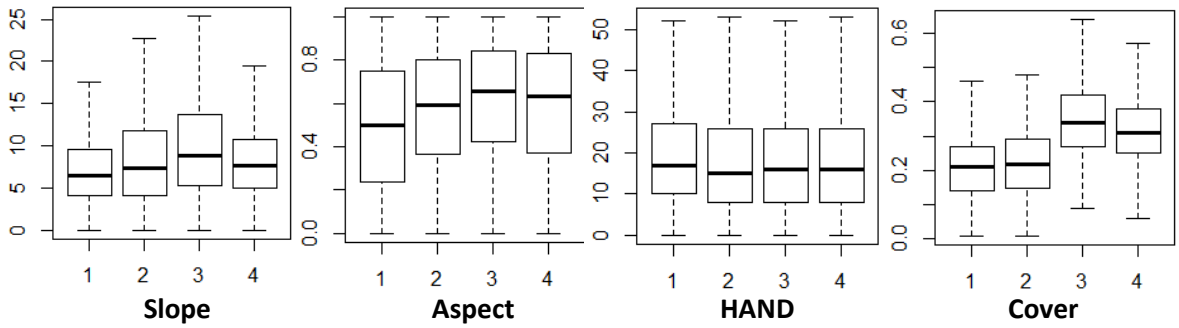

Figure 4.1.6. Boxplots of the slope (degrees), aspect (from 0 (South) to 1 (North)), height above nearest drainage (HAND (m)) and vegetation cover (0-1) for four classes of temporal trends of spatial C_v. Each boxplot corresponds to one of the four classes in section 4.1.3. Cover (cov) and C_v can either have an increasing (+) or decreasing temporal trend (–). 1. cov - C_v + 2. cov + C_v - 3. cov - C_v - 4. cov + C_v + .

Boxplots were also made to study the influence of environmental factors on combined trends in temporal C_v and vegetation cover. Again, cover shows the largest differences between classes. The mean of classes with a positive relationship (3 and 4) between temporal C_v and cover is considerably higher. Here the mean aspect and slope are lower for classes with a negative relationship between temporal C_v and cover (1 and 2).

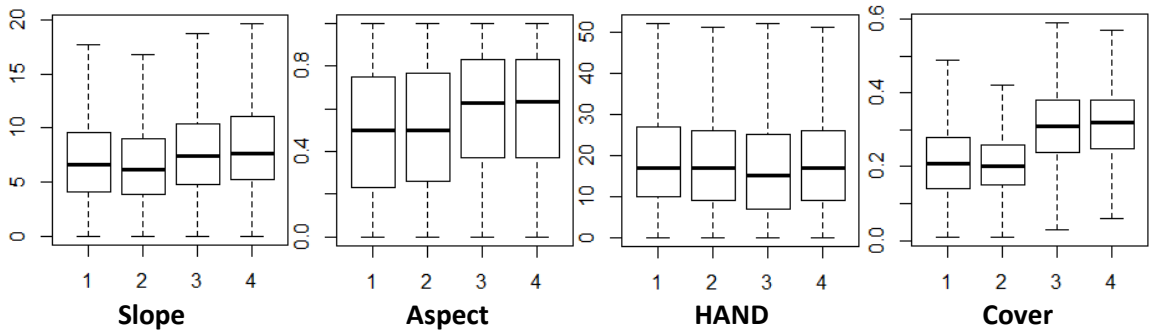

Figure 4.1.7. Boxplots of the slope (degrees), aspect (from 0 (South) to 1 (North)), height above nearest drainage (HAND (m)) and vegetation cover (0-1) for four classes of temporal trends of temporal C_v. Each boxplot corresponds to one of the four classes in section 4.1.3. Cover (cov) and C_v can either have an increasing (+) or decreasing temporal trend (–). 1. cov - C_v + 2. cov + C_v - 3. cov - C_v - 4. cov + C_v +

4.2. Field data

4.2.1 Relations between early warning signals and vegetation in the field

To determine if early warning signals could be measured in the field vegetation cover and spatial variation calculated from the field transects were used. There was a wide range in vegetation cover in these field measurements (table 4.2.1).

Table 4.2.1. Descriptive statistics of vegetation cover (fraction) and C_v (no unit) measured using 24 500m field transects. (n=1104).

	Cover	C_v
Min	0.18	0.02
Mean	0.55	0.24
Max	0.97	0.67
Stdev	0.16	0.11

A regression was run between spatial C_v from a moving window over the transects and vegetation cover measured in the field. A negative correlation coefficient *r* of -0.46 was calculated (p-value 2E-60). The scatterplot (figure 4.2.1.) shows a higher concentration of points when nearing full cover and more spreading out in lower cover.

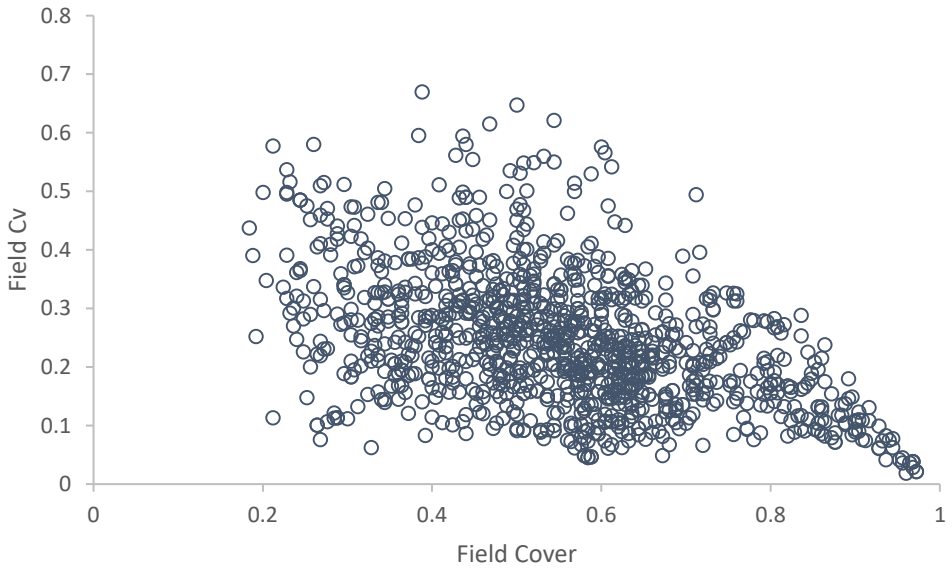

Figure 4.2.1. Scatterplot between cover and spatial C_v of the 2010 transects (n=1104).

4.2.2 Comparing field surveyed to remotely sensed early warning signals

NDVI was compared against vegetation cover measured in the field to see if vegetation cover can be accurately measured using remote sensing. The insignificant correlation coefficient was 0.11 (*p*-value 0.46). However, some outliers can be seen at the right of the scatterplot (figure 4.2.2).

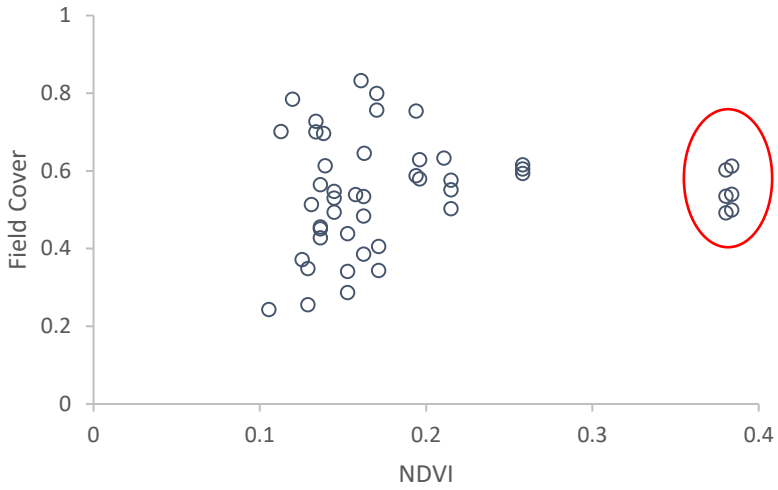

Figure 4.2.2. Scatterplot between cover from the 24 transects and remotely sensed NDVI. Lecina points in red circle.

These outliers were given a closer visual inspection. All the outliers were near the village of Lecina. The points used to extract these outlier values were within 30 meters of a cultivated field (figure 4.2.3). This means a Landsat pixel includes the cultivated field in the reflectance of these points and are therefore not reliable. The regression was run again without these points and the correlation coefficient was 0.25 (*p*-value 0.11).

Table 4.2.2. Descriptive statistics of vegetation cover (fraction) and C_v measured using 24 500m field transects and remotely sensed spatial C_v, NDVI and MSDI (no units) without the Lecina points. (n=42).

	NDVI	Field Cover	Remote C_v	Field C_v	MSDI
Min	0.11	0.24	0.07	0.15	0.05
Mean	0.16	0.54	0.23	0.24	0.15
Max	0.26	0.83	0.48	0.41	0.30
Stdev	0.04	0.15	0.11	0.06	0.06

Figure 4.2.3. Points near Lecina used to extract values from the satellite image.

To study the relationship between remotely sensed spatial C_v and vegetation cover measured in the field they were compared and correlated without the Lecina points (figure 4.2.4.). There was no significant correlation 0.007 (*p*-value 0.96). Part of the points in the scatterplot seem to form a negative trendline, but there are a lot of points with low spatial C_v values.

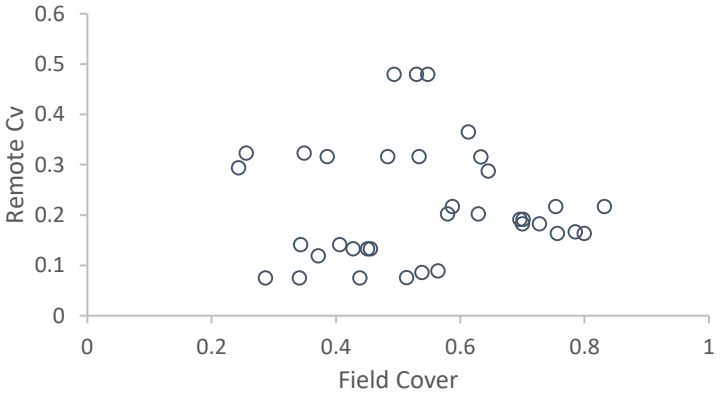

Figure 4.2.4. Scatterplot between cover measured at the transects and remotely sensed spatial C_v.

To compare spatial C_v against MSDI as an early warning signal a regression was run between remotely sensed MSDI and cover measured in the field. There was a moderate positive correlation of 0.41 (*p*-value 0.003), while spatial C_v did not have a significant correlation. The MSDI scatterplot was more linear and elongated.

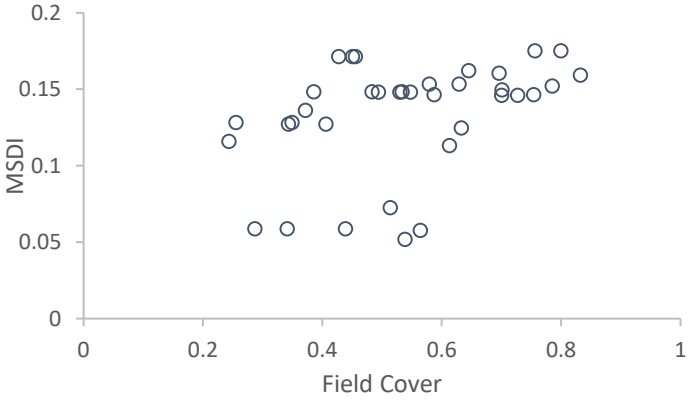

Figure 4.2.5. Scatterplot between cover measured at the transects and remotely sensed MSDI.

Remotely sensed early warning signals were compared against early warning signals measured in the field. Remotely sensed spatial C_v was plotted and correlated against spatial C_v measured in the field and the correlation found was 0.47 (p-value 0.03). So, while remotely sensed spatial C_v and vegetation cover measured in the field showed no correlation there was a correlation between field measured and remotely sensed spatial C_v.

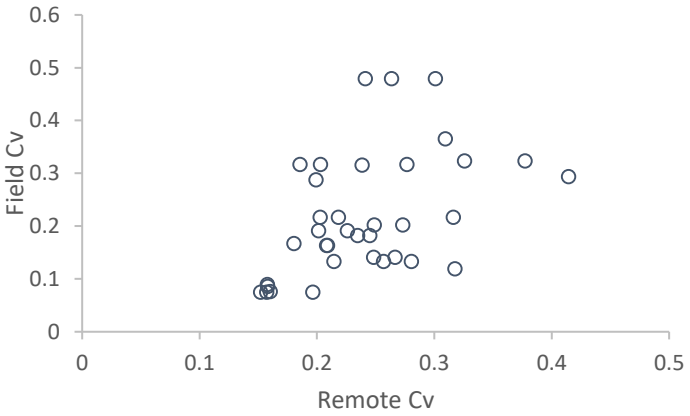

Figure 4.2.6. Scatterplot between spatial C_v from the transects and remotely sensed spatial C_v.

5. Discussion & conclusion

Early warning signals of desertification were calculated using vegetation cover derived from SMA and NDVI. Spatial and temporal $C_v$were used as early warning signals. Trends over time were calculated for these early warning signals and vegetation cover. A classification between four classes for spatial C_v and four classes for temporal C_v could be made by combining these trends with vegetation cover. Spatial $C_v$was also calculated for 24 transects measuring vegetation cover in the field. The remotely sensed spatial C_v and vegetation cover were then compared to spatial C_v and vegetation cover measured in the field.

The most important result is that remotely sensed spatial $C_v$has a moderate to strong (-0.49) negative correlation with vegetation cover calculated using SMA. This means it could possibly be used as an early warning signal for a critical shift from vegetated to a bare state, because vegetation cover can be used as a proxy for ecosystem health (Vicente-Serrano et al., 2012). Spatial C_v also had a stronger negative correlation than the positive correlation (0.29) of MSDI with vegetation cover. This expected negative correlation between C_v (spatial and temporal) and vegetation cover exists in about 80% of the study area. Xu et al. (2009) had a comparable success ratio of 90% using MSDI over the whole Ordos plateau in China. Tanser and Palmer (1999) had moderate to strong correlation between their measure of spatial variance MSDI and NDVI. However out of their five plots in South Africa three had a negative correlation and two had a positive correlation. The unpredictability of the relation between vegetation cover and MSDI makes it less useful than Spatial $C_v$as an early warning signal. Jafari et al. (2008) measured MSDI near watering holes in South Australia and concluded that spatial variance was significantly lower the further away from the degraded areas, which is in line with this study. Guo et al. (2004) also found significantly higher MSDI in grazed areas. Both Jafari et al. (2008) and Guo et al. (2004) did not calculate correlations. While NDVI is strongly correlated to vegetation cover (0.91) its correlation with spatial $C_v$was much weaker (-0.19). This could be due to the higher effectiveness of using spectral mixture analysis in regions with patchy shrub vegetation such as the study area (Elmore et al., 2000).

Spatial C_v is for both the NDVI and SMA better correlated than temporal C_v. Guttal and Jayaprakash (2009) also found in model studies that spatial variation was more reliable than temporal variation. This might be due to a heterogenous environment where temporal variation as an indicator for a critical shift is less suitable (Dakos et al., 2009). Temporal C_v as it is calculated per pixel does not have the smoothing effect spatial C_v has due to its moving window. Together with patchy shrub vegetation this will result in a highly heterogenous early warning signal from one pixel to the next. This will make it harder to locate larger areas in danger of a critical shift. So, while both spatial and temporal C_v can be used as an early warning signal of desertification, spatial C_v is better suited.

The four classes of different combined trends over time between spatial and temporal C_v and vegetation cover seem to differ between different areas. This could be due to differences in environmental factors. Especially cover, slope and aspect (in that order) show differences in mean between classes. Cover and slope also differ in maximum values between classes. This could at least in part explain the spatial distribution of combined trends in vegetation cover and spatial and temporal C_v. Vicente-Serrano et al (2012) only looked at trends in vegetation cover but concluded that decreases in vegetation cover occurred in areas with low water availability and already low vegetation cover. It would be expected that spatial $C_v$would increase in areas with lower water availability as these areas are more at risk of a critical shift. While areas with higher water availability would have a decrease in spatial C_v. This seems to be the case.

In field data the same significant moderate to strong negative correlation (-0.46) between spatial C_v and vegetation cover was found. Spatial C_v was generally higher in areas that had grazing which is expected due to the higher pressure on the ecosystem. This means early warning signals of desertification can be measured in the field. It would be useful if a remotely sensed early warning signal of desertification would correlate to field measurements of vegetation cover to remotely map desertification. Due to the low overlap between the remote sensing cover data and the field data NDVI was used to compare. There was no significant correlation between remotely sensed spatial C_v and vegetation cover in the field. This could be due to the use of NDVI which showed no significant correlation with vegetation cover measured in the field. MSDI did have a correlation with cover measured in the field (0.47). However, there was a moderate to strong correlation (0.46) between remotely sensed spatial C_v and spatial C_v measured in the field. So early warning signals in the field are comparable to remotely sensed early warning signals.

The use of Google Earth Engine made it possible to analyse and process large quantities of satellite and secondary data. It would be relatively easy to apply the techniques described in this thesis to different areas or even on a global scale. This would make it possible to monitor other dryland areas for spatial variation as an early warning signal. Testing if the correlation found between with spatial $C_v$and vegetation cover in the Ebro basin are the same elsewhere. An increase in drought episodes along the Mediterranean basin and the related increased stress on vegetation warrants an early warning system that covers larger areas (Gouveia et al., 2017).

6. References

Agencia Estatal de Meteorología. 2016. Standard climate Values: Zaragoza Aeropuerto - Agencia Estatal de Meteorología - AEMET. Gobierno de España. Available at http://www.aemet.es/en/serviciosclimaticos/datosclimatologicos/valoresclimatologicos?l=9434&k=arn (verified 10 October 2016).

Balbontín, J., V. Penteriani, and M. Ferrer. 2003. Variations in the age of mates as an early warning signal of changes in population trends? The case of Bonelli's eagle in Andalusia. Biological Conservation 109(3): 417–423.

Biggs, R., S.R. Carpenter, and W.A. Brock. 2009. Turning back from the brink: Detecting an impending regime shift in time to avert it. PNAS 106(3): 826–831.

Carpenter, S.R., J.J. Cole, M.L. Pace, R. Batt, W.A. Brock, T. Cline, J. Coloso, J.R. Hodgson, J.F. Kitchell, D.A. Seekell, L. Smith, and B. Weidel. 2011. Early Warnings of Regime Shifts: A Whole-Ecosystem Experiment. Science 332(6033): 1079–1082.

Dakos, V., E.H. van Nes, R. Donangelo, H. Fort, and M. Scheffer. 2009. Spatial correlation as leading indicator of catastrophic shifts. Theor Ecol 3(3): 163–174.

Drake, J.M., and B.D. Griffen. 2010. Early warning signals of extinction in deteriorating environments. Nature 467(7314): 456.

Dregne, H., M. Kassas, and B. Rozanov. 1991. A new assessment of the world status of desertification. Desertification Control Bulletin (20): 6–18.

Elmore, A.J., J.F. Mustard, S.J. Manning, and D.B. Lobell. 2000. Quantifying Vegetation Change in Semiarid Environments: Precision and Accuracy of Spectral Mixture Analysis and the Normalized Difference Vegetation Index. Remote Sensing of Environment 73(1): 87–102.

FAO. 1987. Committee on Agriculture, Improving Productivity of Dryland Areas, Rome.

Fensholt, R., K. Rasmussen, P. Kaspersen, S. Huber, S. Horion, and E. Swinnen. 2013. Assessing Land Degradation/Recovery in the African Sahel from Long-Term Earth Observation Based Primary Productivity and Precipitation Relationships. Remote Sensing 5(2): 664–686.

Google. 2010. Google Earth Engine. Available at https://earthengine.google.com/ (verified 19 September 2017).

Gorelick, N., M. Hancher, M. Dixon, S. Ilyushchenko, D. Thau, and R. Moore. 2017. Google Earth Engine: Planetary-scale geospatial analysis for everyone. Remote Sensing of Environment.

Gouveia, C.M., R.M. Trigo, S. Beguería, and S.M. Vicente-Serrano. 2017. Drought impacts on vegetation activity in the Mediterranean region: An assessment using remote sensing data and multi-scale drought indicators. Global and Planetary Change 151(Supplement C): 15–27.

Guo, X., J. Wilmshurst, S. McCanny, P. Fargey, and P. Richard. 2004. Measuring spatial and vertical heterogeneity of grasslands using remote sensing techniques. Journal of Environmental Informatics 3(1): 24–32.

Guttal, V., and C. Jayaprakash. 2008. Changing skewness: an early warning signal of regime shifts in ecosystems. Ecology Letters 11(5): 450–460.

Guttal, V., and C. Jayaprakash. 2009. Spatial variance and spatial skewness: leading indicators of regime shifts in spatial ecological systems. Theor Ecol 2(1): 3–12.

Jafari, R., M.M. Lewis, and B. Ostendorf. 2008. An image-based diversity index for assessing land degradation in an arid environment in South Australia. Journal of Arid Environments 72(7): 1282–1293.

Karssenberg, D., and M.F.P. Bierkens. 2012. Early-warning signals (potentially) reduce uncertainty in forecasted timing of critical shifts. Ecosphere 3(2): 1–22.

Karssenberg, D., M.F.P. Bierkens, and M. Rietkerk. 2017. Catastrophic Shifts in Semiarid Vegetation-Soil Systems May Unfold Rapidly or Slowly. The American Naturalist 190(6): E145–E155.

Kassas, M. 1995. Desertification: a general review. Journal of Arid Environments 30(2): 115–128.

Kéfi, S., V. Guttal, W.A. Brock, S.R. Carpenter, A.M. Ellison, V.N. Livina, D.A. Seekell, M. Scheffer, E.H. van Nes, and V. Dakos. 2014. Early Warning Signals of Ecological Transitions: Methods for Spatial Patterns. PLOS ONE 9(3): e92097.

Kéfi, S., M. Rietkerk, C.L. Alados, Y. Pueyo, V.P. Papanastasis, A. ElAich, and P.C. de Ruiter. 2007. Spatial vegetation patterns and imminent desertification in Mediterranean arid ecosystems. Nature 449(7159): 213–217.

López-Moreno, J.I., E. Morán-Tejeda, S.M. Vicente Serrano, J. Lorenzo-Lacruz, and J.M. García-Ruiz. 2011. Impact of climate evolution and land use changes on water yield in the Ebro basin.

Lu, D., and M. Batistella. 2005. Exploring TM image texture and its relationships with biomass estimation in Rondônia, Brazilian Amazon. Acta Amazonica 35(2): 249–257.

Ministerio de Agricultura, Alimentación y Medio Ambiente (MAPA). 1978. Mapa de Cultivos y Aprovechamientos de España.

MMA. 2006. Spanish National Forestry Map.

Montanarella, L., and G. Tóth. 2008. Desertification in Europe. *In* 15th International Congress of the International Soil Conservation (ISCO Congress) Soil and Water Conservation, Climate Change and Environmental Sensitivity. Citeseer.

Munyati, C., and D. Makgale. 2009. Multitemporal Landsat TM imagery analysis for mapping and quantifying degraded rangeland in the Bahurutshe communal grazing lands, South Africa. International Journal of Remote Sensing 30(14): 3649–3668.

Nicholson, S.E., C.J. Tucker, and M. Ba. 1998. Desertification, drought, and surface vegitation: An example from the West African Sahel. Bulletin of the American Meteorological Society 79(5): 815.

Nobre, A.D., L.A. Cuartas, M. Hodnett, C.D. Rennó, G. Rodrigues, A. Silveira, M. Waterloo, and S. Saleska. 2011. Height Above the Nearest Drainage – a hydrologically relevant new terrain model. Journal of Hydrology 404(1): 13–29.

Park, C.-E., S.-J. Jeong, M. Joshi, T.J. Osborn, C.-H. Ho, S. Piao, D. Chen, J. Liu, H. Yang, H. Park, B.-M. Kim, and S. Feng. 2018. Keeping global warming within 1.5 °C constrains emergence of aridification. Nature Climate Change 8(1): 70.

Paudel, K.P., and P. Andersen. 2010. Assessing rangeland degradation using multi temporal satellite images and grazing pressure surface model in Upper Mustang, Trans Himalaya, Nepal. Remote Sensing of Environment 114(8): 1845–1855.

Pueyo, Y., D. Moret-Fernández, H. Saiz, C.G. Bueno, and C.L. Alados. 2013. Relationships Between Plant Spatial Patterns, Water Infiltration Capacity, and Plant Community Composition in Semi-arid Mediterranean Ecosystems Along Stress Gradients. Ecosystems 16(3): 452–466.

Rietkerk, M., S.C. Dekker, P.C. de Ruiter, and J. van de Koppel. 2004. Self-Organized Patchiness and Catastrophic Shifts in Ecosystems. Science 305(5692): 1926–1929.

Scheffer, M., J. Bascompte, W.A. Brock, V. Brovkin, S.R. Carpenter, V. Dakos, H. Held, E.H. van Nes, M. Rietkerk, and G. Sugihara. 2009. Early-warning signals for critical transitions. Nature 461(7260): 53–59.

Scheffer, M., S. Carpenter, J.A. Foley, C. Folke, and B. Walker. 2001. Catastrophic shifts in ecosystems. Nature 413(6856): 591–596.

Scheffer, M., S.R. Carpenter, T.M. Lenton, J. Bascompte, W. Brock, V. Dakos, J. van de Koppel, I.A. van de Leemput, S.A. Levin, E.H. van Nes, M. Pascual, and J. Vandermeer. 2012. Anticipating Critical Transitions. Science 338(6105): 344–348.

SITAR. 2007. Geología, Centro de Documentación e Información territorial de Ara.

Soriano, M.A., J.L. Simon, J. Gracia, and T. Salvador. 1994. Alluvial sinkholes over gypsum in the Ebro basin (Spain): genesis and environmental impact. Hydrological Sciences Journal 39(3): 257–268.

Symeonakis, E., and N. Drake. 2004. Monitoring desertification and land degradation over sub-Saharan Africa. International Journal of Remote Sensing 25(3): 573–592.

Tanser, F.C., and A.R. Palmer. 1999. The application of a remotely-sensed diversity index to monitor degradation patterns in a semi-arid, heterogeneous, South African landscape. Journal of Arid Environments 43(4): 477–484.

Tirabassi, G., J. Viebahn, V. Dakos, H.A. Dijkstra, C. Masoller, M. Rietkerk, and S.C. Dekker. 2014. Interaction network based early-warning indicators of vegetation transitions. Ecological Complexity 19: 148–157.

UNCED. 1992. Rio Declaration on Environment and Development.

USGS. 2006. Shuttle Radar Topography Mission.

Vicente-Serrano, S.M., and J.M. Cuadrat-Prats. 2006. Trends in drought intensity and variability in the middle Ebro valley (NE of the Iberian peninsula) during the second half of the twentieth century. Theor. Appl. Climatol. 88(3–4): 247–258.

Vicente-Serrano, S.M., J.M. Cuadrat-Prats, and A. Romo. 2006. Aridity influence on vegetation patterns in the middle Ebro Valley (Spain): Evaluation by means of AVHRR images and climate interpolation techniques. Journal of Arid Environments 66(2): 353–375.

Vicente-Serrano, S.M., T. Lasanta, and A. Romo. 2004. Analysis of Spatial and Temporal Evolution of Vegetation Cover in the Spanish Central Pyrenees: Role of Human Management. Environmental Management 34(6): 802–818.

Vicente-Serrano, S.M., A. Zouber, T. Lasanta, and Y. Pueyo. 2012. Dryness is accelerating degradation of vulnerable shrublands in semiarid Mediterranean environments. Ecological Monographs 82(4): 407–428.

Westing, A.H. 1994. Population, Desertification, and Migration. Environmental Conservation 21(2): 110–114.

Xu, D., X. Kang, D. Qiu, D. Zhuang, and J. Pan. 2009. Quantitative Assessment of Desertification Using Landsat Data on a Regional Scale – A Case Study in the Ordos Plateau, China. Sensors (Basel) 9(3): 1738–1753.